Threshold-Free Symbol Decision Based on Spatial 4PPM Correlation for Uplink Screen Camera Communication Using Low-Luminance SDM Screen

Alisa Kawade, Wataru Chujo, *Life Member, IEEE*, and Kentaro Kobayashi, *Member, IEEE*

***Abstract*—In uplink screen camera communication from a smartphone screen to an indoor telephoto camera at a distance of 3.5 meters, low-luminance space division multiplexing screen is used to increase bitrate and enhance physical layer security (PLS) at wide angles. Since the low-luminance pixels on the screen are affected by ambient light, it is difficult to determine each cell symbol correctly using pre-trained pixel value threshold. To make symbol decisions without threshold learning, symbol decisions based on correlation of spatial 4 pulse position modulation (4PPM) pattern are demonstrated with numerical models and experiments. To increase bitrate further, threshold-free symbol decision methods combining 4PPM and inverted 4PPM cells are demonstrated. In addition, to enhance PLS at wide angles while maintaining error-free transmission in the front direction, threshold-free symbol decision methods are analyzed and experimentally verified at wide angles.**

***Index Terms*—Optical camera communication, physical layer security, pulse position modulation, screen camera communication, space division multiplexing, threshold-free, visible light communication.**

I. Introduction

VISIBLE light communication (VLC) differs from radio-wave communication in that the communication range of light is limited to short distances and the range can be visually perceived. In addition, optical camera communication (OCC), which uses a camera as a receiver, can simultaneously obtain a wide field of view and high spatial resolution in VLC. These properties make OCC superior to radio-wave communication in terms of interference immunity and security. OCC is promised to develop as a means to complement radio-wave communication by utilizing properties different from those of radio waves [1], [2], [3], [4].

In the application of OCC, downlink OCC has been widely studied because it can utilize existing LED lightings [5], [6] and display screens [7], [8] as transmitters and smartphone cameras as receivers. On the other hand, there are few studies for uplink OCC which uses small light source as a transmitter and telephoto camera as a receiver. By taking advantage of the interference immunity and security, uplink OCC can realize personal authentication such as smartphone payment in limited areas, production management in a factory, and communication tools in a hospital. In addition, uplink OCC is available for full-duplex communication combined with the downlink. From the point of view of these OCC applications, it is important to realize uplink OCC.

As a transmitter for uplink OCC, a smartphone screen is most suitable to increase bitrate because the screen consists of large number of pixels. In uplink screen camera communication (SCC) composed of a smartphone screen and an indoor telephoto camera, it can increase bitrate with space division multiplexing. Although downlink SCC, which uses a large screen as a transmitter, has been extensively studied [7], [8], [9], [10], [11], [12], there are no studies on uplink SCC using a small screen other than smartphone-to-smartphone SCC [13], [14], [15].

Generally, in downlink SCC using a large display screen, transmission distance is not much longer than the screen size. On the other hand, in uplink SCC using a small screen, transmission distance is much longer than the screen size. An indoor uplink SCC with a relatively long distance of 3.5 meters has been demonstrated [16]. Space division multiplexing (SDM) screen consists of low-luminance on-off keying (OOK) cells. As the distance increases or the screen cell size decreases, it becomes difficult to focus the camera on the screen. Spatial inter-symbol interference (ISI) due to camera's defocus blur degrades the captured SDM image.

To overcome the spatial ISI, adaptive thresholding, which considers the surrounding 8-cell OOK pattern, was demonstrated [17], [18]. The adaptive thresholding sets the optimal threshold for a central cell with each outer 8-cell pattern in 3 $\times$ 3 cells. Although the outer 8-cell pattern is estimated from a conventional fixed threshold, the pattern helps to determine the threshold adaptively.

OOK adaptive thresholding effectively determines the threshold for symbol decision. However, the adaptive thresholding needs to learn the appropriate threshold using known cell patterns in advance. As the number of cells on the screen increases, the spatial ISI increases, making it difficult to set an appropriate threshold. As the screen luminance decreases, the ambient light makes it difficult to uniquely determine the threshold.

Manuscript received 13 January 2024; revised 25 April 2024; accepted 10 May 2024. Date of publication 14 May 2024; date of current version 21 May 2024. This work was supported by JSPS KAKENHI under Grant JP24K07484. *(Corresponding author: Wataru Chujo.)*

The authors are with the Department of Electrical and Electronic Engineering, Meijo University, Nagoya 468-8502, Japan (e-mail: 213427010@ccalumni.meijo-u.ac.jp; wchujo@meijo-u.ac.jp; kkobaysh@meijo-u.ac.jp).

Digital Object Identifier 10.1109/JPHOT.2024.3400877

Threshold-free symbol decision methods that determine the symbol without pre-trained pixel value threshold are required.

In this study, to improve the robustness of SDM symbol decision against spatial ISI and ambient light, correlation coefficient of spatial 4-pulse position modulation (4PPM) is used for threshold-free symbol decision. SDM symbol decision with spatial 4PPM correlation is compared to that with OOK adaptive thresholding.

Furthermore, uplink SCC needs to be more secure than the downlink. This security is classified as a countermeasure against man-in-the-middle (MITM) attacks among the potential attack vectors. To improve the security, it is necessary to enhance physical layer security (PLS) at wide angles in addition to encryption with upper layer protocols. Since the communication range of uplink SCC is limited to short distances, PLS for SCC at wide angles is inherently higher than that for radio-wave communication [19]. However, PLS needs to be further enhanced against MITM attacks to prevent symbol information on the SDM screen from being intercepted by unauthorized cameras at wide angles. Several studies have been conducted on PLS enhancement for short-range SCC, where the smartphone screen and camera are facing each other with a distance of about 10 cm [13], [20], [21]. However, no studies have been conducted on PLS enhancement for long-distance SCC.

In our previous studies, PLS has been enhanced by increasing spatial ISI at wide angles using SDM screens composed of low-luminance OOK cells [16]. To enhance PLS at wide angles, bit error rate (BER) needs to be very high at wide angles while BER needs to be very low at narrow angles in front. However, in OOK-based SDM, low-luminance screen is affected by ambient light. It is difficult to meet both BER conditions at narrow angles in front and at wide angles. For PLS enhancement under ambient light conditions, threshold-free symbol decision methods that achieve ideal BER performances both in the front direction and at wide angles are required. In this study, to enhance PLS at wide angles while maintaining error-free transmission in the front direction, spatial 4PPM correlation is used for threshold-free symbol decision.

The rest of the paper is organized as follows. In Section II, principle of spatial 4PPM correlation is described, and in Section III, numerical analysis for SDM with spatial 4PPM correlation is given. Section IV presents experimental results of SDM with spatial 4PPM correlation. In Section V, numerical analysis for wide-angle PLS with spatial 4PPM correlation is given. Section VI presents experimental results of wide-angle characteristics with spatial 4PPM correlation. Section VII summarizes conclusions and future work.

II. Principle of Spatial 4PPM Correlation

Fig. 1 shows schematic diagram of indoor uplink SCC using a smartphone screen and an indoor telephoto camera with a relatively long distance of 3.5 meters. A 600 × 1200-pixel screen consists of $n \times m$ SDM cells.

Fig. 2(a) and (b) shows partial 3 × 3-cell arrangements of OOK on the smartphone screen and the camera image, respectively. Let the pixel values on the screen be p_i. The pixel value of the central cell on the camera, P_0, is given by the coupling

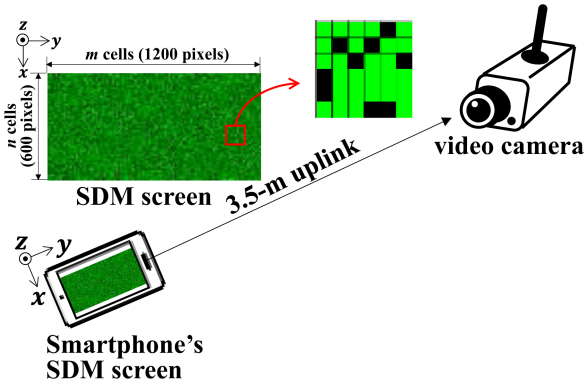

Fig. 1. Schematic diagram of indoor uplink SCC using SDM screen.

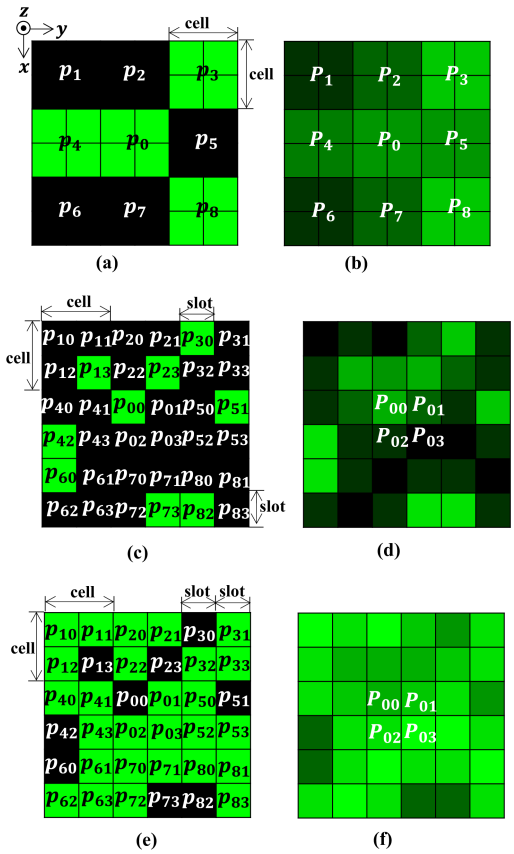

Fig. 2. 3 × 3-cell arrangements on the screen and the camera: (a) OOK on the screen, (b) OOK on the camera, (c) 4PPM on the screen, (d) 4PPM on the camera, (e) I-4PPM on the screen, and (f) I-4PPM on the camera.

from the pixel values, p_i, on the screen owing to the spatial ISI as follows:

$$P_0 = w_{00}p_0 + \sum_{i=1}^{8} w_{0i}p_i \,, \tag{1}$$

where w_{0i} represents the coupling coefficient from the outer 8-cell OOK pattern owing to the spatial ISI. Since $w_{0i}p_i$ is unknown at the receiver, threshold for symbol decision of P_0 is adaptively determined by the outer 8-cell pixel values, P_i.

TABLE I
COMPUTATIONAL COMPLEXITY OF 4PPM CORRELATION

algorithm	processing time ratio
OOK fixed threshold*	1
OOK adaptive threshold*	3
4PPM correlation	4

*Pre-training processing time is not included in OOK threshold.

The optimal threshold for the central cell, P_0 is determined with the outer 8-cell pattern in every 3 × 3 cells [17], [18].

On the other hand, Fig. 2(c), (d), (e), and (f) shows 3 × 3-cell arrangements of 4PPM and inverted 4PPM (I-4PPM) on the smartphone screen and the camera image, respectively. Each cell of 4PPM and I-4PPM consists of four slots. The pixel values of the central cell on the screen are expressed as $(p_{00},\ p_{01},\ p_{02},\ p_{03})$. Spatial 4PPM cell illuminates only one of the four slots, such as $(1,\ 0,\ 0,\ 0)$, and I-4PPM cell illuminates three slots, such as $(0,\ 1,\ 1,\ 1)$. Let pixel values of four slots in the central cell on the camera image be $(P_{00},\ P_{01},\ P_{02},\ P_{03})$. Correlation coefficient, r, between the pixel values on the screen and on the camera is expressed by

$$r = \frac{\sum_{i=0}^{3}\left[\left(p_{0i}-\overline{p_0}\right)\left(P_{0i}-\overline{P_0}\right)\right]}{\sqrt{\sum_{i=0}^{3}\left[\left(p_{0i}-\overline{p_0}\right)^2\right]}\sqrt{\sum_{i=0}^{3}\left[\left(P_{0i}-\overline{P_0}\right)^2\right]}}, \tag{2}$$

where $\overline{p_0}$ and $\overline{P_0}$ represent the average pixel values of the center cell on the screen and camera image, respectively.

Even when using 4PPM or I-4PPM cells, spatial ISI from the surrounding cells affects symbol decision of the central cell. However, symbol decision can be made using correlation coefficient, r, without threshold learning even when the pixel value of low-luminance screen changes with the ambient light.

Computational complexity of 4PPM correlation is compared with that of conventional OOK threshold processing as shown in Table I. In 4PPM correlation, the correlation coefficients with 4-slot patterns are calculated based on (2). Therefore, a total of 12 multiplications are required to calculate 4PPM correlation. However, since the first term in the denominator can be calculated as a constant in advance, the computational complexity is reduced to a total of 8 multiplications. Moreover, since 4PPM transmits 2 bits per symbol, the processing time for 4PPM is simply 4 times that for OOK. On the other hand, in OOK threshold processing, adaptive thresholding is required because the threshold is affected by the surrounding 3 × 3 cell pattern [17], [18]. First, the symbol pattern is coarsely determined assuming a fixed threshold. Next, adaptive thresholds are determined based on the coarsely determined symbol patterns to improve the accuracy of symbol pattern decision. Next, the accuracy of the symbol pattern decision is further increased using adaptive thresholds based on the symbol patterns with increased accuracy. Therefore, the adaptive threshold processing repeats the threshold calculation at least 3 times. As a result, the processing time for 4PPM is only 1.3 times longer than that for OOK adaptive thresholding. The computational complexity of 4PPM correlation is almost the same as that of conventional OOK.

In addition, in OOK symbol decision, pre-training is needed. At least 2^9 different types of known symbols are required for pre-training to categorize 3 × 3 cells.

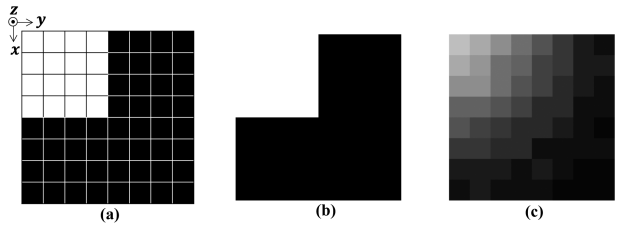

Fig. 3. An example of the analysis model for 4PPM cell using 2D Gaussian function: (a) 8 × 8 pixels/cell model, (b) screen image, and (c) camera image ($\sigma = 3$).

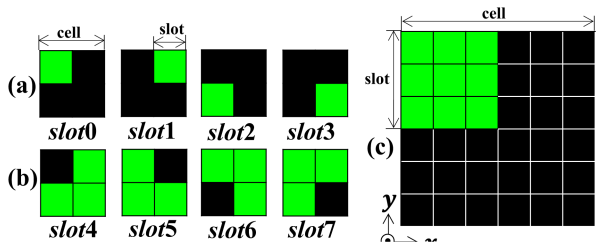

Fig. 4. 4PPM and I-4PPM slot patterns: (a) 4PPM, (b) I-4PPM, and (c) 6 × 6 pixels/cell model.

III. NUMERICAL ANALYSIS FOR SDM WITH SPATIAL 4PPM CORRELATION

A. 4PPM and I-4PPM Correlation

A point spread function (PSF) is utilized as a function representing the response to a point light source. In general, it is difficult to express PSF that accurately describes the defocus blur with a simple function. However, it is known that PSF can be approximated by a two-dimensional (2D) Gaussian function. Fig. 3(a) shows an example of the analysis model of a 4PPM cell consisting of 8 × 8 pixels and expresses (1, 0, 0, 0). The spread of each pixel value on the camera due to defocus blur is given by

$$P\left(x,y\right) = \frac{1}{2\pi\sigma^2}\exp\left(-\frac{x^2+y^2}{2\sigma^2}\right), \tag{3}$$

where σ is the standard deviation that represents the spread of PSF when the pixel spacing is normalized to 1, and x and y represents the position of each pixel on the camera image. Fig. 3(b) and (c) shows an example of the screen and camera image, respectively, where one cell consists of 8 × 8 pixels, expresses (1, 0, 0, 0), and the standard deviation, $\sigma = 3$.

Correlation coefficients of 3 × 3 SDM cells composed of 4PPM or I-4PPM cell are numerically analyzed based on (3). Fig. 4(a) and (b) shows 4PPM and I-4PPM slot patterns. Since each cell consists of four slots, 4PPM has four patterns named *slot0*, *slot1*, *slot2*, and *slot3* and I-4PPM has the patterns named

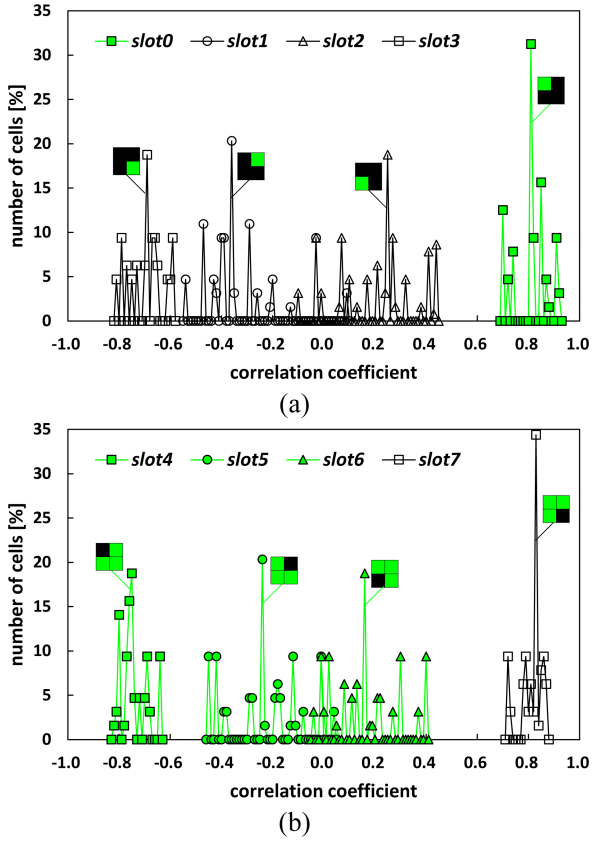

Fig. 5. Correlation coefficients of the central cell in 3 × 3-cell arrangement on the camera image, where each cell consists of 6 × 6 pixels and the standard deviation, $\sigma = 2$: (a) 4PPM correlation with *slot0* pattern and (b) I-4PPM correlation with *slot7* pattern.

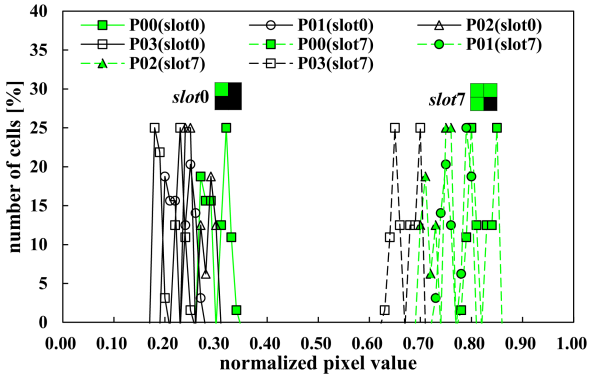

Fig. 6. Pixel value distribution of the central cell in 3 × 3-cell arrangement with 4PPM and I-4PPM cells on the camera image.

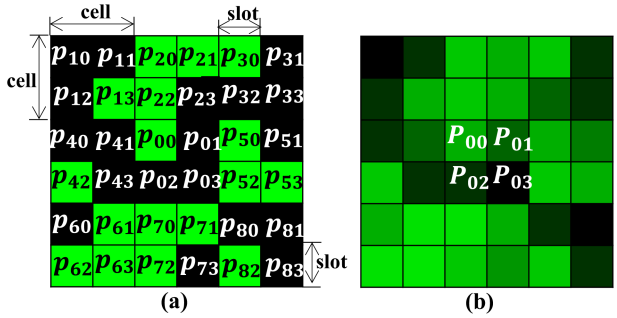

Fig. 7. 3 × 3-cell arrangements of combining 4PPM and I-4PPM cells: (a) On the screen and (b) on the camera.

slot4, *slot5*, *slot6*, and *slot7*, where each cell consists of 6 × 6 pixels as shown in Fig. 4(c).

Fig. 5 shows correlation coefficients of the central cell in 3 × 3-cell arrangement of 4PPM and I-4PPM (See Fig. 2(c)–(f)), where the standard deviation, $\sigma = 2$. In Fig. 5(a) and (b), the central cell of 4PPM and I-4PPM screen transmits *slot0* pattern that expresses (1, 0, 0, 0) and *slot7* pattern that express (1, 1, 1, 0), respectively. Therefore, in Fig. 5(a), *slot0*, *slot1*, *slot2*, and *slot3* show the correlation coefficients between the central cell on the camera image that expresses (1, 0, 0, 0) and the slot patterns on the screen that express (1, 0, 0, 0), (0, 1, 0, 0), (0, 0, 1, 0), and (0, 0, 0, 1), respectively. In the same way, in Fig. 5(b), *slot4*, *slot5*, *slot6*, and *slot7* show the correlation coefficients between the central cell on the camera image that expresses (1, 1, 1, 0) and the slot patterns on the screen that express (0, 1, 1, 1), (1, 0, 1, 1), (1, 1, 0, 1), and (1, 1, 1, 0), respectively.

In Fig. 5(a) and (b), correlation coefficients of *slot0* and *slot7* patterns are the maximum for 4PPM and I-4PPM, respectively. Correlation coefficients with *slot0* and *slot7* patterns do not overlap with other patterns for 4PPM and I-4PPM, respectively. It is possible to determine the correct symbol without pre-trained pixel value threshold.

On the other hand, Fig. 6 shows normalized pixel value distribution of the central cell in 3 × 3-cell arrangement with 4PPM and I-4PPM cells, where the central cell transmits *slot0* pattern that expresses (1, 0, 0, 0) and *slot7* pattern that express (1, 1, 1, 0), respectively. P_{00}, P_{01}, P_{02}, and P_{03} are pixel values of four slots in the central cell, and number of pixels per cell and standard deviation are the same as those in Fig. 5. Since P_{00} overlaps with other P_{01}, P_{02}, and P_{03} in *slot0* pattern and P_{03} overlaps with other P_{00}, P_{01}, and P_{02} in *slot7* pattern, it is difficult to determine correct symbols using pixel value threshold.

B. Combining 4PPM and I-4PPM Correlation

If the size of a 4PPM slot is equal to the size of an OOK cell, bitrate of 4PPM is half of OOK. To increase the bitrate of SDM screen composed of 4PPM cells, 4PPM and I-4PPM cells are combined on the same screen as shown in Fig. 7(a). Fig. 7(b) shows the combined cells on the camera image. Since 4PPM and I-4PPM patterns are randomly arranged (see Fig. 4), combining 4PPM and I-4PPM cells transmit 3 bits per symbol and the bitrate improves to 3/4 of OOK.

Fig. 8(a) shows correlation coefficients of the central cell in 3 × 3-cell arrangement of combining 4PPM and I-4PPM cells, where the central cell transmits *slot0* pattern that expresses (1, 0, 0, 0). Number of pixels per cell and standard deviation are the same as in Fig. 5. Correlation coefficients with *slot0* are almost the maximum. However, coefficients of *slot0* and *slot7* have some overlap. It is difficult to distinguish between 4PPM and I-4PPM symbols with only the correlation coefficient. Therefore, clustering into 4PPM and I-4PPM cells is required

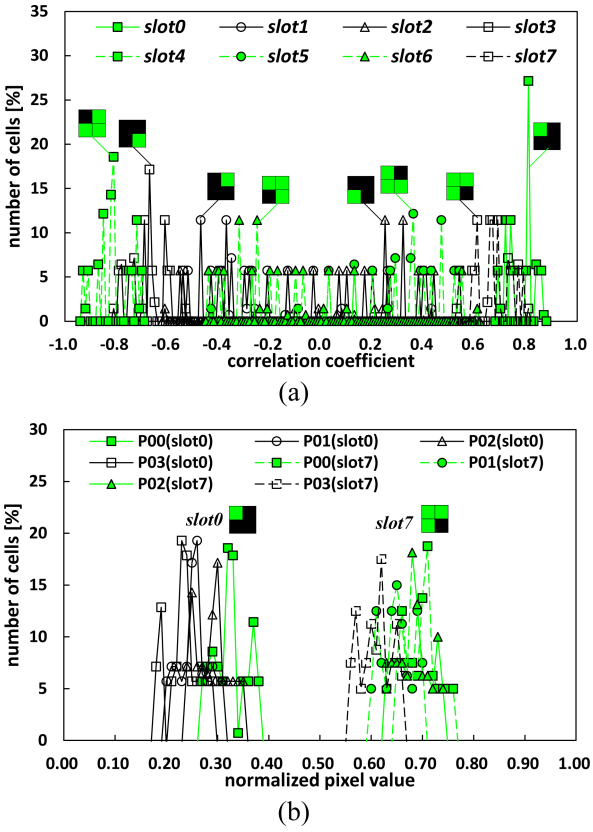

Fig. 8. Correlation coefficients and pixel value distribution of the central cell in 3 × 3-cell arrangement of combining 4PPM and I-4PPM cells on the camera image: (a) Correlation coefficients with *slot0* pattern and (b) pixel value distributions of *slot0* and *slot7* patterns.

before calculating the correlation coefficient of 4PPM and I-4PPM, respectively. The clustering is also an unsupervised learning technique used to find patterns in data without prior knowledge [22].

To realize clustering into 4PPM and I-4PPM cells, Fig. 8(b) shows pixel value distributions of *slot0* and *slot7* patterns, where the central cell transmits *slot0* and *slot7* patterns. Even when both patterns are combined, *slot0* and *slot7* patterns can be clustered with pixel values without pre-trained pixel value threshold. Since the luminance of I-4PPM cells is much different from that of 4PPM cells, pixel value distributions are not much affected by combining 4PPM and I-4PPM cells. The difference in average pixel values between 4PPM and I-4PPM cells are used to cluster into 4PPM and I-4PPM cells without threshold learning. Since the differences in received pixel values are used to cluster into 4PPM and I-4PPM cells before calculating the correlation coefficients, it is possible to correlate only with 4PPM or I-4PPM cells after the clustering.

IV. Experimental Results of SDM With Spatial 4PPM Correlation

A. Measurement Specifications

To verify the numerical analysis of 4PPM and I-4PPM correlation, experiments on spatial 4PPM correlation were conducted.

TABLE II
Measurement Specifications

smartphone screen	
frame rate	15 frames per second
image resolution	2448×1080 pixels (Full HD+)
refresh rate	144 Hz
screen pixel value	green, 0-255
smartphone	ASUS ROG Phone 5

video camera	
frame rate	30 frames per second
image resolution	1920×1080 pixels
Lens focal length	4.4-88 mm
image sensor pixel value	green, 0-255
video camera	SONY FDR-AX60

Bit error rate (BER) for SDM transmission using spatial 4PPM correlation was compared with that using OOK adaptive thresholding. Table II shows measurement specifications for indoor uplink SCC at a long distance of 3.5 meters. The green pixel value on the screen is as low as possible to realize low-luminance luminance SDM transmission. A time series of SDM screen images consisting of square cells with specific green pixel values such as 63, 53, and 47 are created using OpenCV-python (See a 600 × 1200-pixel screen in Fig. 1). Pseudo-random binary sequence 28 (PRBS28) is used to generate random data. The screen images are displayed continuously on the screen at 15 frames per second using animation created in Android Studio. BER was measured indoors under fluorescent lighting.

B. BER Comparison

To accurately compare 4PPM correlation and OOK adaptive thresholding, BERs for 4PPM and OOK cells with the same bitrates were measured. Fig. 9 shows BERs for 4PPM, I-4PPM, combining 4PPM and I-4PPM, and OOK measured while decreasing green pixel value on the screen to 63, 53, and 47. In 4PPM and I-4PPM cells, only correlation coefficients were used for threshold-free symbol decision. In combining 4PPM and I-4PPM cells, correlation coefficients and clustering with pixel value distribution were used for symbol decision without threshold learning. On the other hand, in OOK, adaptive threshold that determines symbols by pre-trained pixel value threshold was used.

Fig. 9(a) shows BER versus bitrate, where green pixel value on the screen is 63. Combining 4PPM and I-4PPM without threshold learning can achieve lower BER than OOK adaptive thresholding at the same bitrate. In addition, Fig. 9(b) shows BER when green pixel value on the screen is 53. As the green pixel values on the screen decrease, combining 4PPM and I-4PPM correlation without threshold learning achieves much lower BER than OOK adaptive thresholding at the same bitrate. Spatial 4PPM correlation is more tolerant of pixel value variations due to ambient light than OOK adaptive thresholding. Moreover, Fig. 9(c) shows BER when green pixel value on the

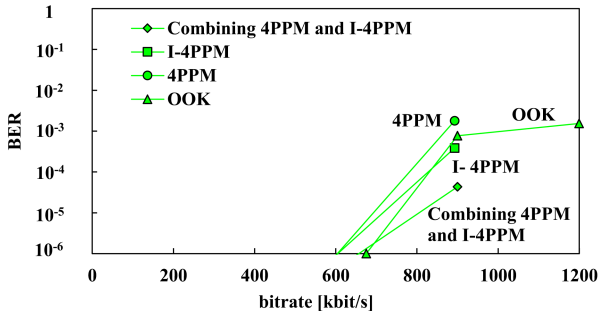

(a)

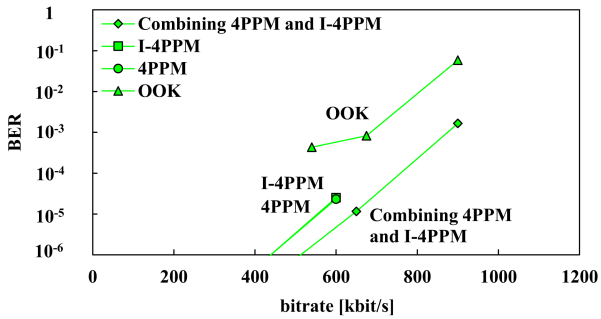

(b)

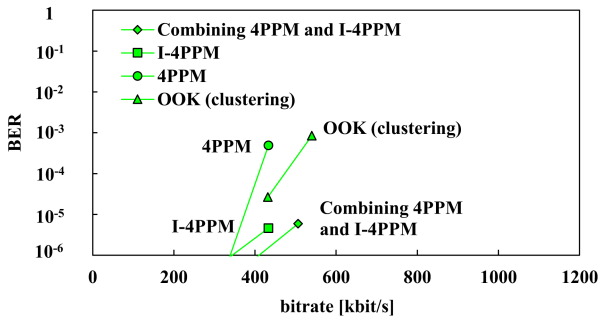

(c)

Fig. 9. BER versus bitrate: (a) Green pixel value on the screen is 63 and (b) 53, (c) 47.

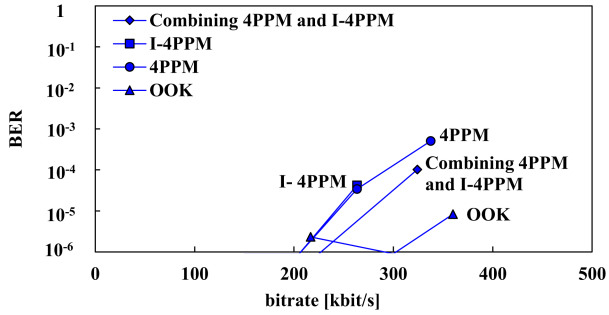

(a)

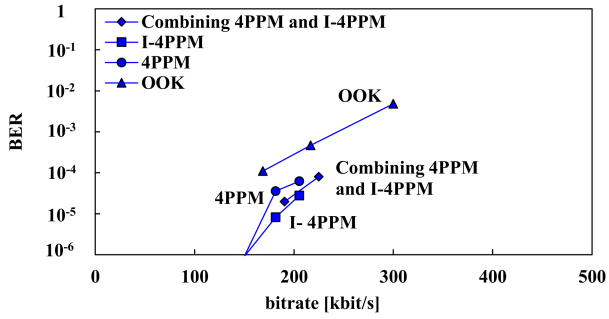

(b)

Fig. 10. BER versus bitrate: (a) Blue pixel value on the screen is 73 and (b) 63.

screen is 47. Since OOK adaptive thresholding no longer works due to strong influence of ambient light, clustering with received pixel values is used to determine OOK symbols instead of adaptive thresholding. However, combining 4PPM and I-4PPM correlation achieves much lower BER than OOK clustering at the same bitrate. Combining 4PPM and I-4PPM achieved BER of less than 10^{-6} at 506 kbps and 392.04 kbps when green pixel value on the screen is 53 and 47 respectively.

To validate the robustness of the spatial 4PPM correlation, the cell color on the screen was changed from green to blue. Fig. 10 shows BERs for 4PPM, I-4PPM, combining 4PPM and I-4PPM, and OOK measured while decreasing blue pixel value on the screen to 73 and 63. Fig. 10(a) shows BER versus bitrate, where blue pixel value on the screen is 73. Since the blue pixel value on the screen is still high, OOK adaptive thresholding achieves lower BER than 4PPM, I-4PPM, and combining 4PPM and I-4PPM. On the other hand, when blue pixel value on the screen decreases to 63, combining 4PPM and I-4PPM without threshold learning can achieve lower BER than OOK adaptive thresholding at the same bitrate. Even when using blue cells instead of green cells, spatial 4PPM correlation is more tolerant of pixel value variations due to ambient light than OOK adaptive thresholding.

C. 4PPM Correlation and Clustering With Pixel Values

Details of 4PPM correlation and clustering with pixel values are revealed. Fig. 11(a) and (b) shows measured correlation coefficients of combining 4PPM and I-4PPM with *slot0* and *slot7* patterns, where green pixel value on the screen is 53 and bitrate is 506 kbps. Since the correlation coefficients of *slot0* and *slot7* have some overlap with each other, differences between the average pixel values of *slot0* and *slot7* are used to cluster into 4PPM and inverted 4PPM cells. Fig. 11(c) and (d) shows measured pixel value distributions of *slot0* and *slot7*. Although pixel value distributions have some overlap due to ambient light, differences in average pixel values in small areas were compared as details below.

Fig. 12(a) shows three-dimensional (3D) pixel value distribution of combining 4PPM and I-4PPM on the camera image when green pixel value on the screen is 53. *X* and *Y* axis shows each cell number on the camera and vertical axis shows the average pixel value of each cell. There are large variations in green pixel values on the camera image due to ambient light. However, it is clearly shown that 4PPM and I-4PPM cells can be clustered if limited to a narrow area.

To clarify the difference between the average green pixel values of 4PPM and I-4PPM cells, Fig. 12(b) shows the average

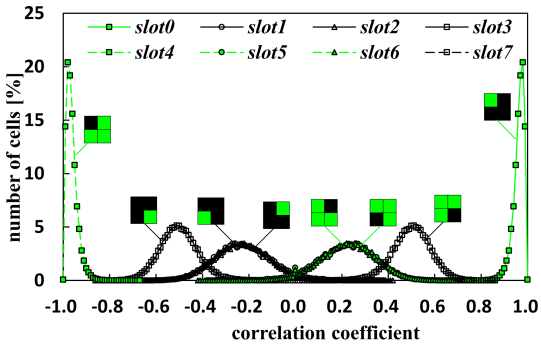

(a)

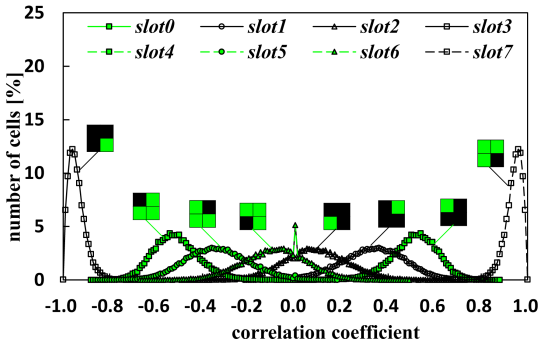

(b)

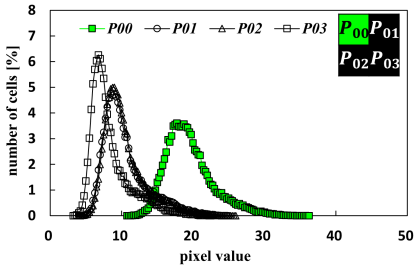

(c)

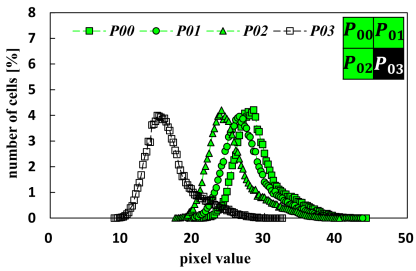

(d)

Fig. 11. Measured correlation coefficients and pixel value distributions of combining 4PPM and I-4PPM cells: (a) Correlation coefficients with *slot0* pattern, (b) *slot7* pattern, (c) pixel value distribution of *slot0* pattern, and (d) *slot7* pattern.

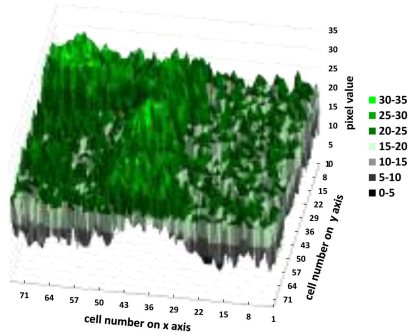

(a)

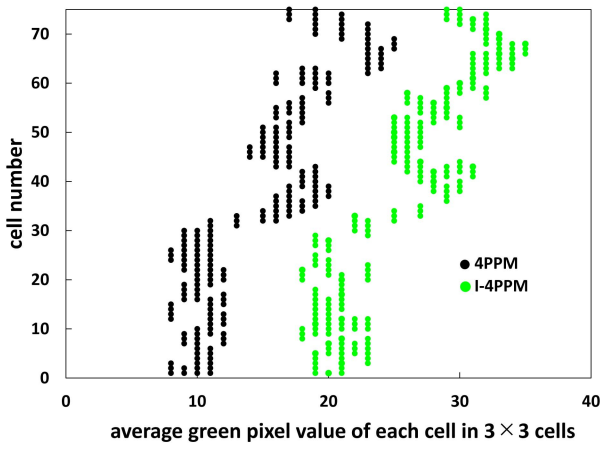

(b)

Fig. 12. Pixel value distribution of combining 4PPM and I-4PPM cells on the camera image when green pixel value on the screen is 53: (a) 3D green pixel value distribution and (b) average green pixel value of each cell in 3×3 cells in which the center cell is located on line $Y = 15$ of the camera image.

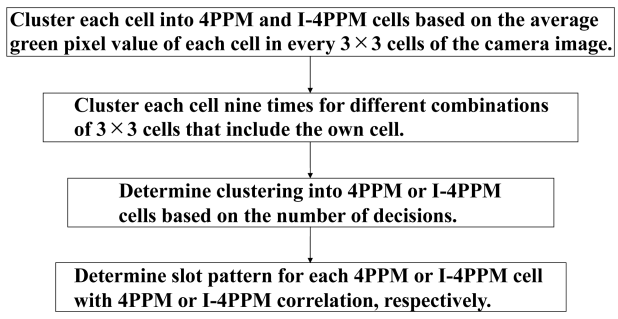

Fig. 13. Symbol decision procedure for combining 4PPM and I-4PPM cells.

green pixel value of each cell in 3×3 cells in which the center cell is located on line $Y = 15$ of the camera image. Since the average green pixel value of 4PPM and I-4PPM cells varies due to ambient light, the average green pixel values overlap in the entire camera image. However, when comparing the average green pixel value of each cell within 3×3 cells, it is clear that the average green pixel values can be clustered into 4PPM and I-4PPM cells.

Fig. 13 shows symbol decision procedure for combining 4PPM and I-4PPM cells. First, each cell in every 3×3 cells of the camera image is clustered into 4PPM and I-4PPM cells based on the average green pixel values of every 3×3 cells. Next, each cell is clustered nine times for different combinations of 3×3 cells that include the own cell. Next, clustering into 4PPM

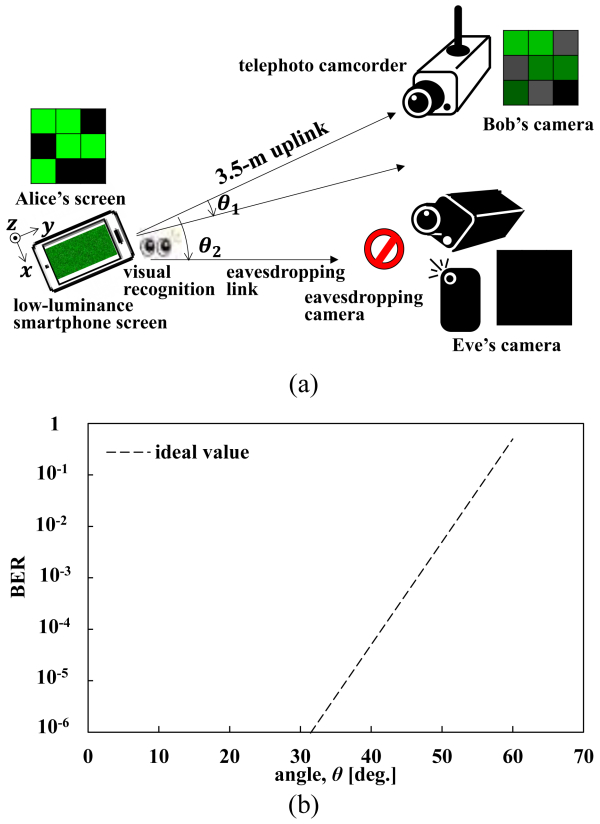

Fig. 14. Model of 3.5 m indoor uplink SCC to enhance PLS at wide angles: (a) Schematic diagram and (b) ideal BER characteristics.

or I-4PPM cells is finally determined based on the number of decisions. After clustering into 4PPM and I-4PPM cells, slot pattern for each 4PPM or I-4PPM cell is determined with 4PPM or I-4PPM correlation, respectively.

V. Numerical Analysis for Wide Angle Physical Layer Security of SDM With Spatial 4PPM Correlation

A. Numerical Model for Wide Angle Characteristics

To prevent MITM attacks in terms of potential attack vectors, enhancement of wide-angle physical layer security (PLS) of low-luminance SDM screen was investigated using spatial 4PPM correlation. Fig. 14(a) shows schematic diagram of long-distance 3.5 m indoor uplink SCC using SDM screen to enhance PLS at wide angles.

In the uplink from Alice's screen to Bob's camera, error-free transmission is required within the angle θ_1. In addition, PLS needs to be enhanced at wide angles more than θ_1 to prevent symbol information on the SDM screen from being intercepted using Eve's camera. Eve's camera needs to be unable to capture Alice's screen at the angles more than θ_1. In fact, it is difficult to rapidly change BER from 0 to 1 when the angle becomes more than θ_1. However, Alice can visually perceive Eve's eavesdropping camera with her own eyes up to θ_2. Therefore, Eve's camera needs to be unable to capture Alice's screen at the angles more than θ_2.

In this study, the angle θ_1 is set to 30° because of the alignment error of the smartphone screen due to Alice's handheld. On the other hand, the angle θ_2 is set to 60° at which Alice cannot visually perceive Eve's eavesdropping camera with her own eyes. Fig. 14(b) shows the ideal BER value that satisfies the wide-angle characteristics for PLS enhancement, where BER is assumed to increase linearly from the angle $\theta_1$to θ_2.

The spread of each pixel luminance on the screen at $\theta = 0^\circ$ is given by (3). In the numerical model for wide-angle characteristics, (3) is modified for wide angles. Consider the case where the screen is tilted by an angle θ in the x-axis direction (see Fig. 14(a)). According to Lambert's cosine law, the received pixel value on the camera decreases with $\cos\theta$. In addition to Lambert's cosine law, SDM screen utilizes the increase in spatial ISI at wide angle, θ, to enhance PLS.

When the screen is tilted by an angle θ in the x-axis direction, standard deviations of the spread of Gaussian function in the x- and y-axis directions are given by $\sigma_x = \sigma/\cos\theta$ and $\sigma_y = \sigma$, respectively. The standard deviation in the x-axis direction, σ_x increases as the angle, θ, increases.

Equation (3) is modified for wide angles as

$$p(x,y) = \frac{\cos\theta}{2\pi\sigma^2/\cos\theta} \exp\left\{-\frac{1}{2}\left(\frac{x^2}{(\sigma/\cos\theta)^2} + \frac{y^2}{\sigma^2}\right)\right\}, \tag{4}$$

where the standard deviation, $\sigma = 2$ is the same as Section III. Also, in the numerical model for wide-angle characteristics, the same 4PPM cell with 6×6 pixels per cell and 3×3 SDM cells as Section III are used (see Figs. 2(c) and 4(c)).

B. Simulation Results

Wide-angle characteristics of correlation coefficients of 3×3 SDM cells composed of 4PPM or I-4PPM alone and combined 4PPM and I-4PPM cells are numerically analyzed based on (4). Fig. 15 shows wide-angle characteristics of 4PPM correlation coefficients of the central cell in 3×3-cell arrangement, where the standard deviation, $\sigma = 2$ (see Figs. 2(c) and 4(c)).

Fig. 15(a) shows the correlation coefficients at $\theta = 30^\circ$. Although the correlation coefficients of the *slot0* pattern and the other patterns are close, correct symbol decision is still possible. In contrast, Fig. 15(b) shows the correlation coefficient at $\theta = 60^\circ$. Correlation coefficients of the *slot0* pattern almost overlap with the correlation coefficients of the other 4PPM patterns. It is impossible to determine the symbols correctly.

Wide-angle characteristics of I-4PPM correlation coefficients are almost the same as those of 4PPM correlation coefficients. Correct symbol decision based on I-4PPM correlation coefficients is possible up to $\theta = 30^\circ$. Fig. 16 shows wide angle characteristics of normalized pixel value distribution of the central cell in 3×3-cell arrangement with 4PPM (*slot0*) and I-4PPM (*slot7*), where all the parameters other than θ are the same as those in Fig. 6. Fig. 16(a) and (b) shows pixel value distribution at $\theta = 30^\circ$ and 60°, respectively. Since pixel values of four slots overlap each other in *slot0* and *slot7*, it is impossible to determine the correct symbol based on pixel value distribution.

Moreover, Fig. 17 shows wide-angle characteristics of combining 4PPM and I-4PPM correlation coefficients and pixel

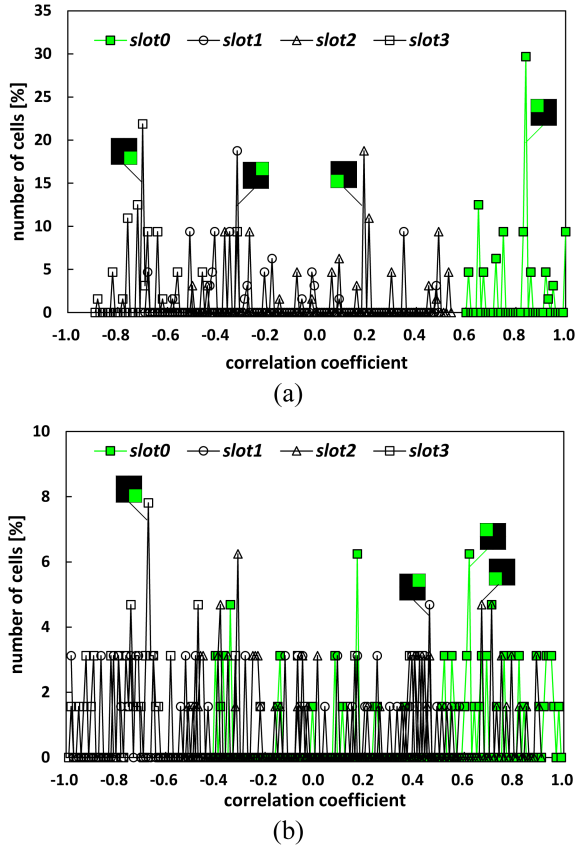

Fig. 15. Wide-angle characteristics of 4PPM correlation coefficient distribution with *slot0* pattern: (a) $\theta = 30°$ and (b) $60°$.

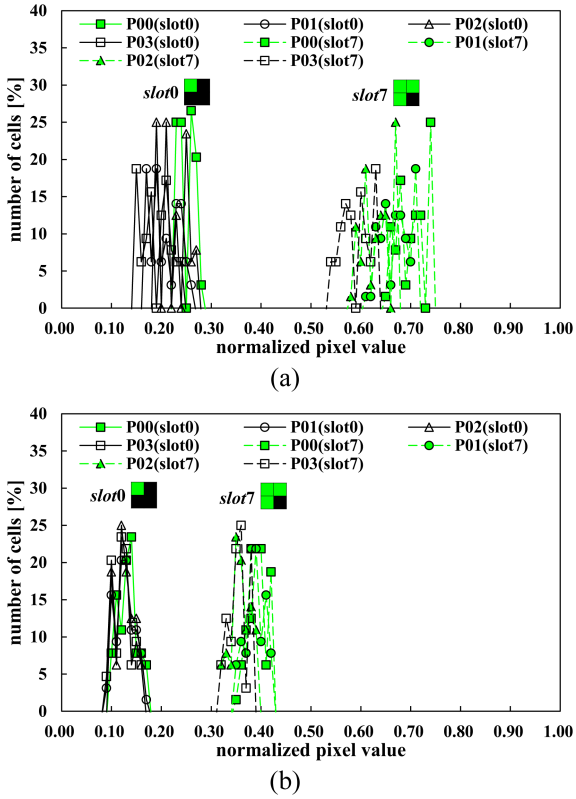

Fig. 16. Wide-angle characteristics of pixel value distribution of the central cell in 3 × 3-cell arrangement with 4PPM (*slot0*) and I-4PPM (*slot7*): (a) $\theta = 30°$ and (b) $60°$.

value distribution of the central cell in 3 × 3-cell arrangement, where the standard deviation, $\sigma = 2$ (see Figs. 4(a), (b) and 7(a)).

Fig. 17(a) shows the correlation coefficients at $\theta = 30°$. The correlation coefficients of *slot0* and *slot7* overlap considerably. Fig. 17(b) shows pixel value distributions at $\theta = 30°$. Pixel values of four slots overlap each other in *slot0* and *slot7*. it is impossible to determine the correct symbol based on pixel value distribution. However, *slot0* and *slot7* patterns are clustered with pixel value distribution. The difference in average pixel values between 4PPM and I-4PPM cells are used to cluster into 4PPM and I-4PPM cells without threshold learning. The clustering of the pixel value distribution into 4PPM and I-4PPM cells allows correct symbol decision in the same way as $\theta = 0°$ (see Fig. 8).

On the other hand, Fig. 17(c) shows the correlation coefficients at $\theta = 60°$. Correlation coefficients of the *slot0* pattern overlap not only with the correlation coefficients of I-4PPM patterns but also the other 4PPM patterns. It is impossible to determine the symbols correctly. Fig. 17(d) shows pixel value distributions at $\theta = 60°$. Since pixel values of four slots in *slot0* and those in *slot7* overlap each other, it is impossible to cluster *slot0* and *slot7* patterns.

These results satisfy the wide-angle characteristics for PLS enhancement, where correct symbol decision is possible up to $\theta = 30°$ and the symbol decision is impossible at $\theta = 60°$.

VI. Experimental Results of Wide-Angle Characteristics of SDM Screen Composed of 4PPM and I-4PPM Cells for PLS Enhancement

A. Wide-Angle Characteristics of I-4PPM Cells

To verify the simulation results, wide-angle characteristics of correlation coefficient distribution and BER were measured using SDM screen composed of I-4PPM cells. Indoor uplink SCC at a long distance of 3.5 meters were conducted while changing the angle, θ. Measurement specifications are the same as those at $\theta = 0°$ (See Table II).

Fig. 18 shows I-4PPM correlation coefficient distribution of *slot7* pattern and BER at wide angles, where green pixel value on the screen is 63, each cell consists of 8 × 8 pixels, each frame consists of 75 × 150 cells, and bitrate is 337.5 kbps. Fig. 18(a) shows the correlation coefficients at $\theta = 0°$. There is a large distance between the correlation coefficients of *slot7* pattern and the other I-4PPM patterns. Fig. 18(b) shows the correlation coefficients at $\theta = 35°$. The correlation coefficients of *slot7* pattern still do not overlap with the correlation coefficients of the other I-4PPM patterns. In contrast, Fig. 18(c) shows the correlation coefficients at $\theta = 60°$. Correlation coefficients of *slot0* pattern almost overlap with the correlation coefficients of the other I-4PPM patterns. It is impossible to determine the symbols correctly.

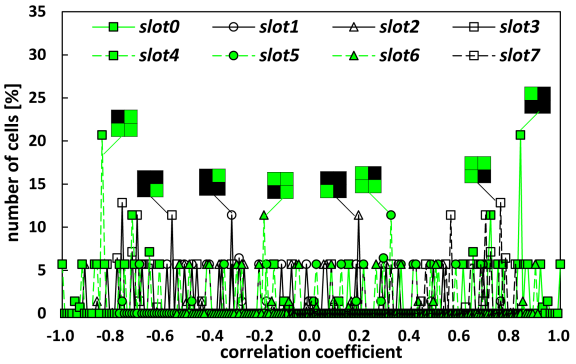

(a)

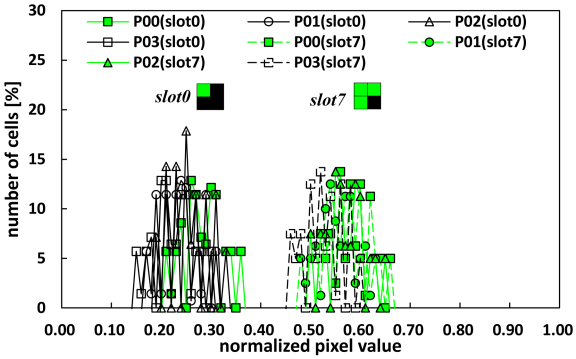

(b)

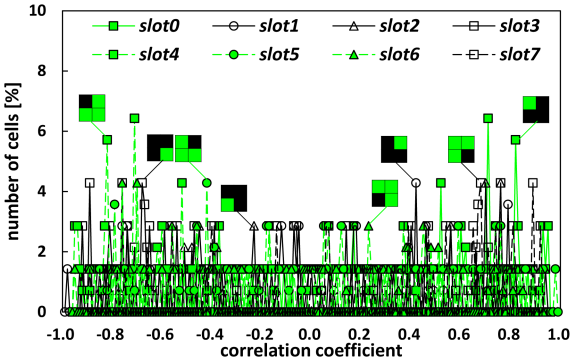

(c)

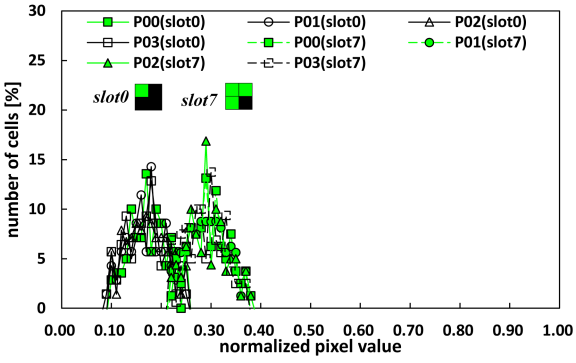

(d)

Fig. 17. Wide-angle characteristics of combining 4PPM and I-4PPM cells: (a) Correlation coefficients at $\theta = 30°$, (b) pixel value distributions at $\theta = 30°$, (c) correlation coefficients at $\theta = 60°$, and (d) pixel value distributions at $\theta = 60°$.

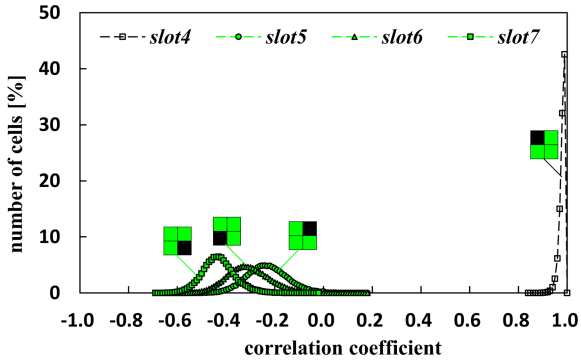

(a)

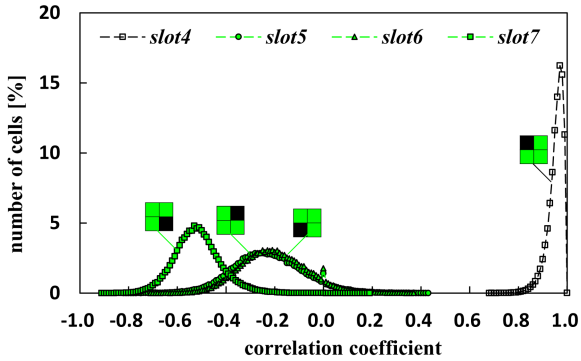

(b)

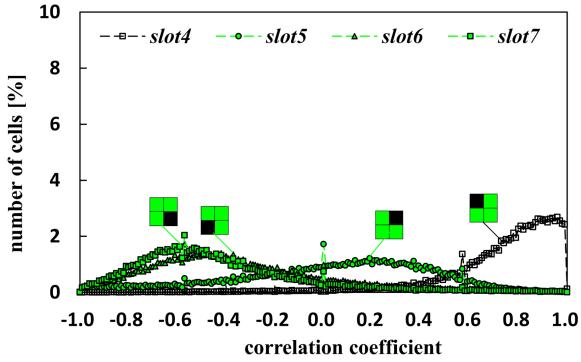

(c)

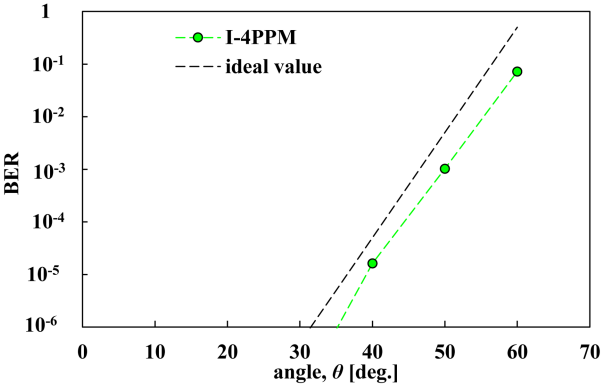

(d)

Fig. 18. Wide-angle characteristics of I-4PPM correlation coefficient distribution of *slot7* pattern and BER: (a) $\theta = 0°$, (b) $35°$, (c) $60°$, and (d) BER.

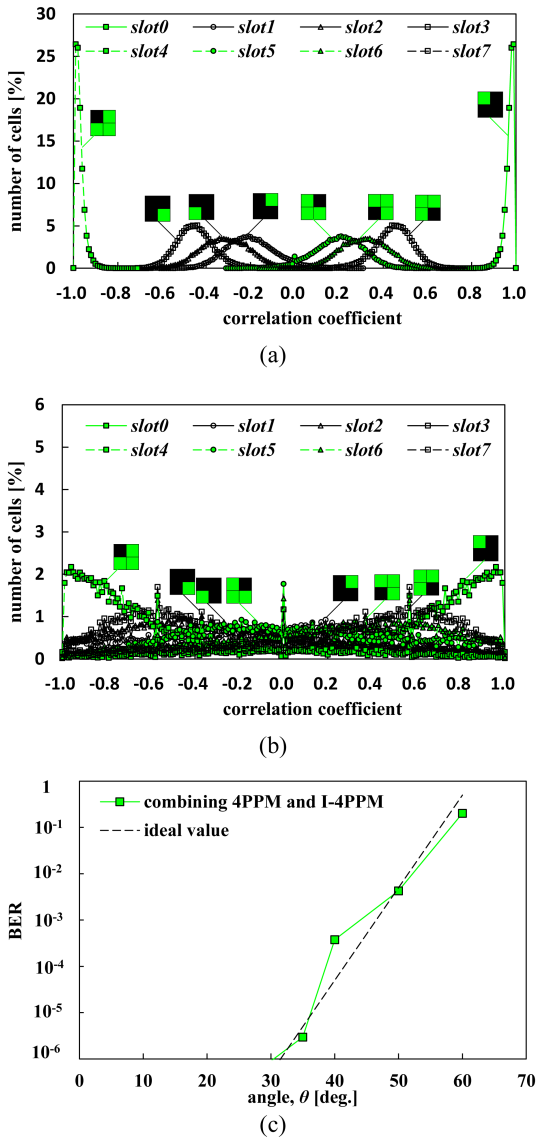

Fig. 19. Wide-angle characteristics of correlation coefficient distribution of *slot0* pattern and BER of combining 4PPM and I-4PPM cells: (a) $\theta = 30°$, (b) 60°, and (c) BER.

Finally, Fig. 18(d) shows wide-angle BER characteristics of I-4PPM cells, where the ideal value shows a straight line connecting the conditions $\theta_1 \leq 30°$ and $\theta_2 \geq 60°$ (see Fig. 14(b)). Pseudo-random binary sequence 28 (PRBS28) was used to generate random data. BERs of less than 10^{-6} are obtained at $\theta_1 \leq 35°$. In addition, BER increases linearly and reaches 10^{-1} at $\theta_2 = 60°$. I-4PPM cells achieve wide-angle BER characteristics close to the ideal value for PLS enhancement without pre-trained pixel value threshold.

B. Wide-Angle Characteristics of Combining 4PPM and I-4PPM Cells

Wide-angle characteristics of correlation coefficient distribution and BER were measured using SDM screen combining 4PPM and I-4PPM cells.

Fig. 19 shows correlation coefficient distribution of *slot0* and BER of combining 4PPM and I-4PPM cells at wide angles, where green pixel value on the screen is 63, each cell consists of 8×8 pixels, each frame consists of 75×150 cells, and bitrate is 506.25 kbps. Fig. 19(a) shows the correlation coefficients at $\theta = 30°$. The correlation coefficients of *slot0* pattern do not overlap with the correlation coefficients of the other 4PPM patterns. However, the correlation coefficients of *slot0* pattern overlap with the correlation coefficients of I-4PPM patterns such as *slot5*, *slot*6, and *slot*7. To cluster into 4PPM and I-4PPM cells, the difference in average pixel values between 4PPM and I-4PPM cells were used. In contrast, Fig. 19(b) shows the correlation coefficients at $\theta = 60°$. Correlation coefficients of *slot0* pattern completely overlap with the correlation coefficients of the other 4PPM and I-4PPM patterns. Even if clustered into 4PPM and I-4PPM cells, it is impossible to determine the symbols correctly.

Fig. 19(c) shows wide-angle BER characteristics of combining 4PPM and I-4PPM cells, where the straight line shows the ideal value for PLS enhancement. Even when combining 4PPM and I-4PPM cells, BERs of less than 10^{-6} are achieved at $\theta_1 \leq 30°$. In addition, BER increases linearly, almost equal to the ideal value, and reaches 10^{-1} at $\theta_2 = 60°$.

VII. Conclusion

Uplink screen camera communication from a smartphone's low-luminance SDM screen to an indoor telephoto camera was demonstrated at a distance of 3.5 meters. To determine symbols without pre-trained pixel value threshold, spatial 4PPM correlation was analyzed and experimentally verified. To further improve bitrate, 4PPM and I-4PPM cells were combined. Pixel value clustering along with 4PPM correlation were utilized for symbol decision without pre-trained pixel value thresholds.

Numerical analysis revealed that correlation coefficients of 4PPM 3×3 cells were clearly separated without learning thresholds, and combining 4PPM and inverted 4PPM cells can be clustered with pixel value distribution. In the experiments, combining 4PPM and I-4PPM correlation achieved much lower BER than OOK adaptive thresholding, and achieved BERs of less than 10^{-6} at 506 kbps when green pixel value on the screen is 53. Bitrate of SDM screen combining 4PPM and I-4PPM cells is 1.5 times higher than that composed of 4PPM or I-4PPM cells. Even when using blue cells instead of green cells on the screen, spatial 4PPM correlation achieved lower BER than OOK adaptive thresholding.

Furthermore, to prevent MITM attacks in terms of potential attack vectors, PLS enhancement for 4PPM screen was demonstrated at wide angles while maintaining error-free transmission in the front direction. Numerical analysis revealed that SDM screen composed of 4PPM cells can utilize increase in spatial ISI at wide angles to enhance PLS. In the experiments, combining 4PPM and I-4PPM cells maintained BERs of less than 10^{-6} at the angles less than 30 deg. and BER increased linearly with increasing angle and reached 10^{-1} at 60 deg., that is close to the ideal value for PLS enhancement.

On the other hand, in terms of simplifying the implementation, a future work is to simplify the alignment of the camera with 4PPM patterns on the screen. Object detection algorithms using

machine learning are interesting for the alignment. The combination of 4PPM correlation and object detection is a promising step to simplify implementation.

REFERENCES

[1] *IEEE Standard for Local and Metropolitan Area Networks-Part 15.7: Short-Range Optical Wireless Communications*, IEEE Standard 802.15.7^{TM}-2018.

[2] H. Abuella et al., "Hybrid RF/VLC systems: A comprehensive survey on network topologies, performance analyses, applications, and future directions," *IEEE Access*, vol. 9, pp. 160402–160436, 2021, doi: 10.1109/ACCESS.2021.3129154.

[3] K. Ali et al., "Measurement campaign on 5G indoor millimeter wave and visible light communications multi component carrier system," *IEEE Trans. Broadcast.*, vol. 68, no. 1, pp. 156–170, Mar. 2022, doi: 10.1109/TBC.2021.3120918.

[4] A. Celik, I. Romdhame, G. Kaddoum, and A. M. Eltawil, "A top-down survey on optical wireless communications for the Internet of Things," *IEEE Commun. Surveys Tuts.*, vol. 25, no. 1, pp. 1–45, Firstquarter 2023, doi: 10.1109/COMST.2022.3220504.

[5] S. Haruyama, "Visible light communication using sustainable LED lights," *Proc. ITU Kaleidoscope: Building Sustain. Communities*, vol. 56, no. 2, pp. 31–36, Apr. 2013.

[6] M. A. Dastgheib, E. Zolala, H. Beyranvand, and J. A. Salehi, "On fundamental limits of energy efficient signaling in visible light communication systems," *IEEE Wireless Commun. Lett.*, vol. 12, no. 10, pp. 1731–1735, Oct. 2023, doi: 10.1109/LWC.2023.3290206.

[7] S. D. Perli, N. Ahmed, and D. Katabi, "PixNet: Interference-free wireless links using LCD-camera pairs," in *Proc. 16th Annu. Int. Conf. Mobile Comput. Netw.*, 2010, pp. 137–148.

[8] Z. Ma, X. Yang, H. Fang, W. Zhang, and N. Yu, "OAcode: Overall aesthetic 2D barcode on screen," *IEEE Trans. Multimedia*, vol. no. 25, pp. 8687–8698, 2023, doi: 10.1109/TMM.2023.3239755.

[9] A. Ashok, S. Jain, M. Gruteser, N. Mandayam, Y. Wenjia, and K. Dana, "Capacity of pervasive camera based communication under perspective distortions," in *Proc. IEEE Int. Conf. Pervasive Comput. Commun.*, 2014, pp. 112–120.

[10] Y. Kim, D. Lee, and D. Kim, "Pre-processing images for enhancing reliability in screen-to-camera communication," *IEEE Wireless Commun. Lett.*, vol. 7, no. 6, pp. 934–937, Dec. 2018, doi: 10.1109/LWC.2018.2839105.

[11] T. Nguyen, M. D. Thieu, and Y. M. Jang, "2D-OFDM for optical camera communication: Principle and implementation," *IEEE Access*, vol. 7, pp. 29405–29424, 2019, doi: 10.1109/ACCESS.2019.2899739.

[12] T. Fujihashi, T. Koike-Akino, P. V. Orlik, and T. Watanabe, "High-throughput visual MIMO systems for screen-camera communications," *IEEE Trans. Mobile Comput.*, vol. 20, no. 6, pp. 2200–2211, Jun. 2021, doi: 10.1109/TMC.2020.2977042.

[13] T. Hao, R. Zhou, and G. Xing, "Cobra: Color barcode streaming for smartphone systems," in *Proc. 10th Int. Conf. Mobile Syst., Appl., Serv.*, 2012, pp. 85–98.

[14] R. Boubezari, H. L. Minh, Z. Ghassemlooy, and A. Bouridane, "Smartphone camera based visible light communication," *J. Lightw. Technol.*, vol. 34, no. 17, pp. 4120–4126, Sep. 2016, doi: 10.1109/JLT.2016.2590880.

[15] M. Stafford, A. Rogers, S. Wu, C. Carver, N. S. Artan, and Z. Dong, "TETRIS: Smartphone-to-smartphone screen-based visible light communication," in *Proc. IEEE 14th Int. Conf. Mobile Ad Hoc Sensor Syst.*, 2017, pp. 570–574.

[16] A. Kawade, W. Chujo, and K. Kobayashi, "Space division multiplexing using high-luminance cell-size reduction arrangement for low-luminance smartphone screen to camera uplink communication," *IEICE Trans. Fundam. Electron., Commun. Comput. Sci.*, vol. E106-A, no. 5, pp. 793–802, May 2023, doi: 10.1587/transfun.2022WBP0004.

[17] A. Kawade, W. Chujo, and K. Kobayashi, "Space division multiplexing by adaptive thresholding for uplink optical camera communication using smartphone screen," *IEICE Commun. Exp.*, vol. 10, no. 12, pp. 954–960, Dec. 2021, doi: 10.1587/comex.2021col0046.

[18] A. Kawade, W. Chujo, and K. Kobayashi, "Two-wavelength adaptive thresholding for uplink from smartphone's low-luminance WDM/SDM screen to camera," *IEICE Commun. Exp.*, vol. 11, no. 7, pp. 441–447, Jul. 2022, doi: 10.1587/comex.2022XBL0074.

[19] M. A. Arfaoui et al., "Physical layer security for visible light communication systems: A survey," *IEEE Commun. Surveys Tust.*, vol. 22, no. 3, pp. 1887–1908, thirdquarter 2020, doi: 10.1109/COMST.2020.2988615.

[20] B. Zhang, K. Ren, G. Xing, X. Fu, and C. Wang, "SBVLC: Secure barcode-based visible light communication for smartphones," *IEEE Trans. Mobile Comput.*, vol. 15, no. 2, pp. 432–446, Feb. 2016, doi: 10.1109/TMC.2015.2413791.

[21] J. Zhao and X.-Y. Li, "Scsec: A secure near field communication system via screen camera communication," *IEEE Trans. Mobile Comput.*, vol. 19, no. 8, pp. 1943–1955, Aug. 2020, doi: 10.1109/TMC.2019.2913412.

[22] C. M. Bihop, *Pattern Recognition and Machine Learning*. Berlin, Germany: Springer-Verlag, 2006.